JMEPEG (2018) 27:4791–4798
https://doi.org/10.1007/s11665-018-3586-1

1059-9495/$19.00

Hot Deformation Behavior of the 20 vol.% TiC/Cu-Al_2O_3 Composites

Yong Liu, Zhiqiang Yang, Baohong Tian, Yi Zhang, Zhengbin Gu, and Alex A. Volinsky

(Submitted January 25, 2018; in revised form June 11, 2018; published online August 27, 2018)

Hot deformation behavior of the 20 vol.% TiC/Cu-Al_2O_3 composite was studied using the Gleeble-1500D thermo-mechanical simulator with various strain rates at different deformation temperatures. The softening mechanism due to dynamic recrystallization was a feature of the high-temperature true stress–strain curves. The peak stress increased at the lower deformation temperature and the higher strain rate. Microstructure evolution was explored. Thermal deformation activation energy was calculated as 218.9 kJ/mol, and the constitutive equation was established. The processing map was constructed to obtain optimal processing domain of 700-850 °C and 0.001-0.04 s^{-1} for hot working.

Keywords constitutive equation, hot compression deformation, processing map, TiC/Cu-Al_2O_3 composite

1. Introduction

Copper is widely used by the power generation industry because of its good electrical conductivity, plasticity and thermal conductivity (Ref 1-4). Titanium carbide is an attractive ceramic compound, which can be used as a reinforcing material of the metallic matrix because of its high modulus, hardness and melting temperature (Ref 5–7). Recently, copper-based metal matrix composites containing TiC particles have been extensively investigated because of their potential applications as electrical sliding contacts, resistance welding electrodes, wear-resistant materials, high-performance switches, rockets throat lining, motors and heat exchangers (Ref 7-9). Al_2O_3 is the most commonly used dispersion strengthening phase, and nanoscale Al_2O_3 prepared by internal oxidation has many advantages. First, the Al_2O_3 particles prepared by internal oxidation can reach nanometer level. Fine Al_2O_3 particles are distributed in the Cu matrix and can maintain good coherency with the matrix. Second, Al_2O_3 can strengthen copper and maintain high conductivity of copper at the same time. Third, the process of Al_2O_3 production by internal oxidation is easy to implement, low in price and convenient for large-scale applications (Ref 10, 11). Copper-based materials have been attracting more attention, especially regarding the research of copper alloys processing technology (Ref 12-15).

During the past few years, properties and microstructure of Cu-TiC composites have been studied (Ref 16-19). However, hot deformation behavior and processing maps of the TiC/Cu-Al_2O_3 composite have not been systematically reported yet. In this paper, hot deformation behavior of the 20 vol.% TiC/Cu-Al_2O_3 composite was studied at various strain rates and different deformation temperatures. The flow stress and microstructure evolution were investigated, and the constitutive equation along with the processing maps was established based on the experimental data.

2. Experiment

Commercial powders of 20 vol.% TiC (48 μm, 99.9% pure), 75 vol.% Cu-0.28%Al (67 μm, 99.9% pure) and 5 vol.% Cu_2O (75 μm, 99.9% pure) were mixed using the QQM/B roller mixer for 12 h. The milled powders were loaded in graphite die and press-sintered in the VDBF-250 vacuum hot pressing sintering furnace at 950 °C under 30 MPa pressure in vacuum (1.8×10^{-2} Pa) for 2 h.

Compression tests were carried out using the Gleeble-1500D thermo-mechanical simulator at 450-850 °C with the strain rate of 0.001-1 s^{-1} and the total strain of 50%. The samples were heated to deformation temperature at 10 °C/s heating rate and then held for 180 s before compression tests. The samples were water-quenched after compression to preserve deformation microstructure, which was characterized by the JSM-5610 LV scanning electron microscope (SEM) and the JEM-2100 high-resolution transmission electron microscope (HRTEM).

Yong Liu, School of Material Science and Engineering, Henan University of Science and Technology, Luoyang 471023, China; Collaborative Innovation Center of Nonferrous Metals, Luoyang 471023 Henan Province, China; and Henan Key Laboratory of Advanced Non-Ferrous Materials, Luoyang 471023, China; **Zhiqiang Yang**, School of Material Science and Engineering, Henan University of Science and Technology, Luoyang 471023, China; **Baohong Tian**, School of Material Science and Engineering, Henan University of Science and Technology, Luoyang 471023, China; and Henan Key Laboratory of Advanced Non-Ferrous Materials, Luoyang 471023, China; **Yi Zhang**, School of Material Science and Engineering, Henan University of Science and Technology, Luoyang 471023, China; and Collaborative Innovation Center of Nonferrous Metals, Luoyang 471023 Henan Province, China; **Zhengbin Gu**, National Laboratory of Solid State Microstructures and Department of Materials Science and Engineering, College of Engineering and Applied Sciences, Nanjing University, Nanjing 210093, China; and **Alex A. Volinsky**, Department of Mechanical Engineering, University of South Florida, Tampa 33620. Contact e-mails: liuyong@haust.edu.cn and volinsky@usf.edu.

3. Results and Discussion

3.1 Initial Microstructure

Figure 1 shows the initial microstructure of the 20 vol.% TiC/Cu-Al_2O_3 composite.

Figure 1(a) shows SEM image of the composite microstructure. Two types of morphological particles can be seen, continuous dense gray dispersed phase of copper matrix and black TiC phase. Figure 1(b) shows HRTEM images of the composite. There are many Al_2O_3 particles ranging from 5 to 20 nm in size. During plastic deformation, nano-sized Al_2O_3 particles can act as dislocation sources, increasing dislocation density. Figure 1(c) is a magnified image of Fig. 1(b). Figure 1(c) illustrates diffuse distribution of Al_2O_3 particles with petal-like morphology and good coherency (Ref 20). Figure 1(d) shows electron diffraction pattern and γ-Al_2O_3 indexing.

3.2 True Stress–Strain Curves

True stress–strain curves of the 20 vol.% TiC/Cu-Al_2O_3 composite obtained at various strain rates and different deformation temperatures are presented in Fig. 2.

Figure 2 shows the effects of deformation temperature and strain rate on the flow stress behavior of the composite. All curves exhibit the same trend of the flow stress increasing quickly to the peak value and then slowly decreasing. This behavior indicates that there is competition between the work hardening and dynamic softening. Work hardening is caused by dislocations multiplication, pileup and tangle. Dynamic softening is caused by dislocations rearrangement and interactions. It can also be seen that the peak stress decreases with deformation temperature. Dynamic recrystallization nucleation rate and growth rate increase with temperature, reinforcing the softening effect, since there are weaker atomic interactions at the higher temperature. It can also be seen that the peak stress increases with the strain rate due to precipitate growth and dislocation slip in a short period of time. Based on these observations, the deformation temperature and strain rate have obvious effects on the flow stress behavior. Thus, the composite is sensitive to the strain rate and deformation temperature.

3.3 Microstructure Analysis

Microstructure of the 20 vol.% TiC/Cu-Al_2O_3 composite at different deformation temperatures with 0.001 s^{-1} strain rate is shown in Fig. 3.

It can be seen that the grains exhibit strong alignment in the deformation direction, resulting in the deformation texture at a relatively low temperature of 450 °C in Fig. 3(a) and 650 °C in Fig. 3(b). However, recrystallized grains can be clearly

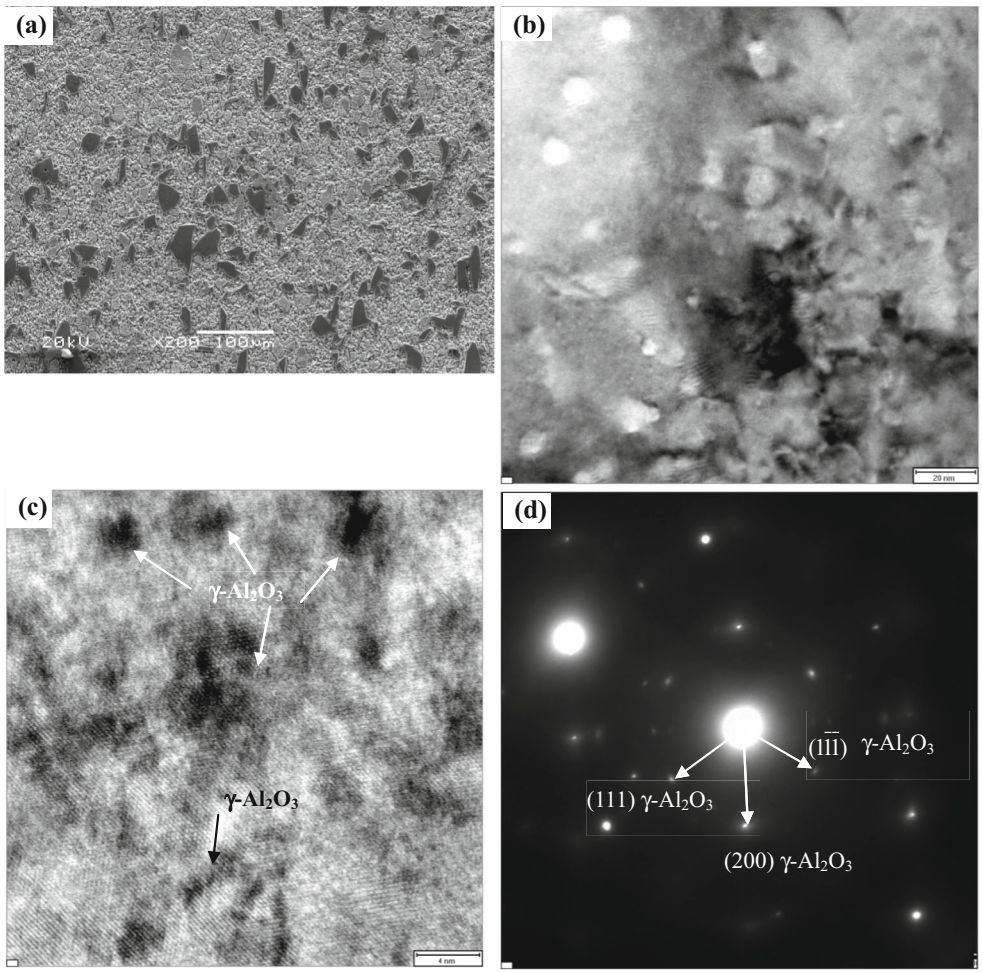

Fig. 1 Initial microstructure of the 20 vol.% TiC/Cu-Al_2O_3 composite: (a) SEM image; (b, c) HRTEM images; (d) selected area electron diffraction pattern and indexing

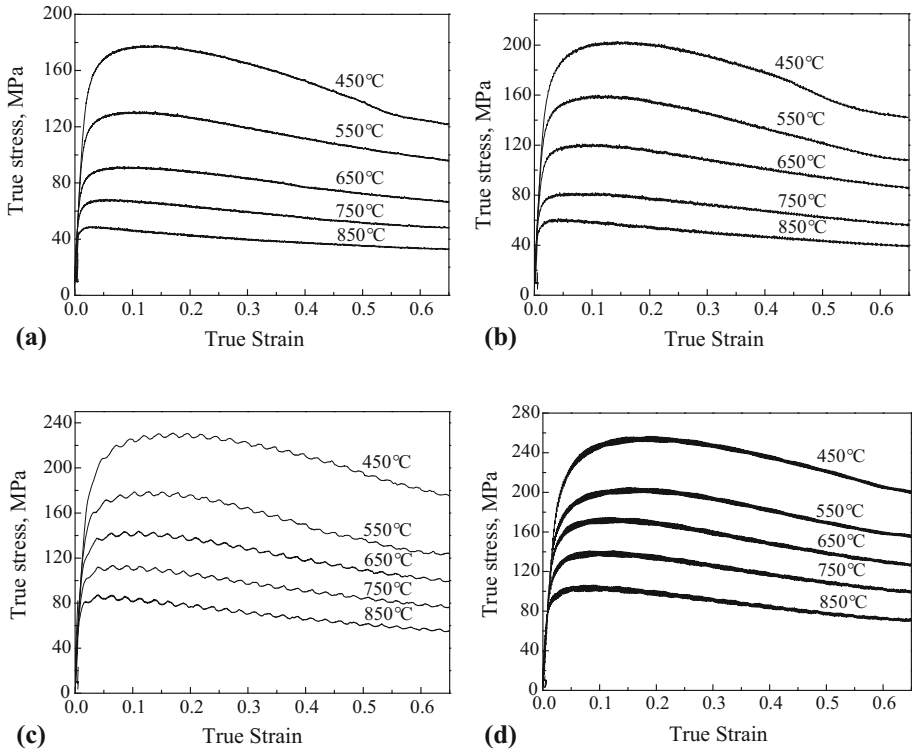

Fig. 2 True stress–strain curves with various strain rates at different temperatures for the 20 vol.% TiC/Cu-Al_2O_3 composite: (a) $\dot{\varepsilon} = 0.001\ s^{-1}$; (b) $\dot{\varepsilon} = 0.01\ s^{-1}$; (c) $\dot{\varepsilon} = 0.1\ s^{-1}$; (d) $\dot{\varepsilon} = 1\ s^{-1}$

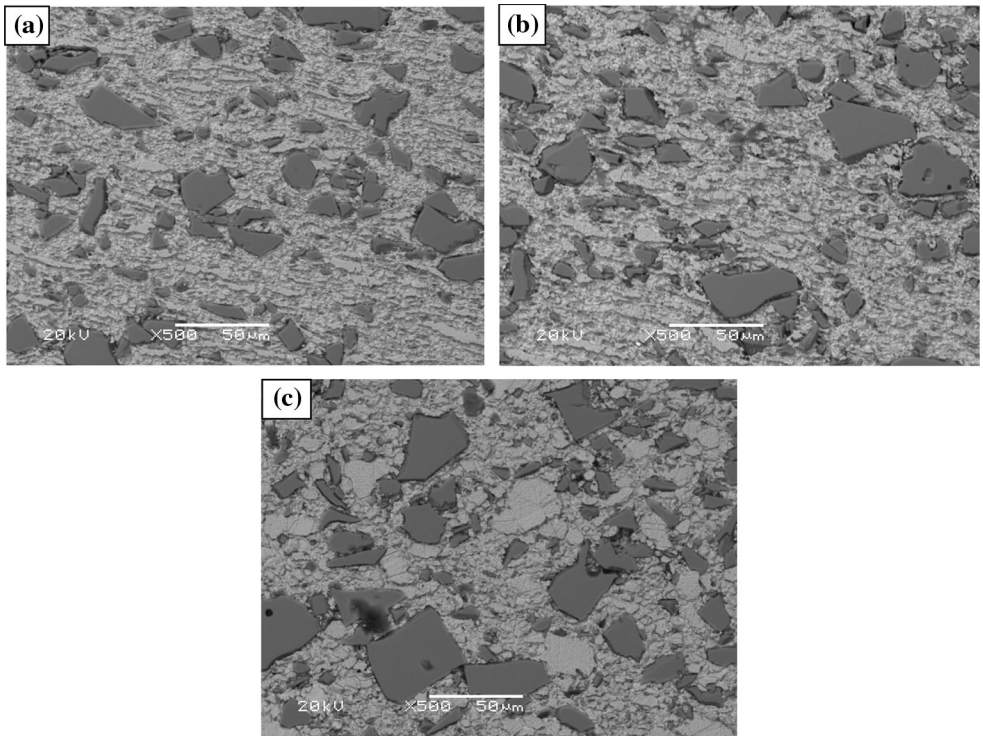

Fig. 3 Microstructure of the 20 vol.% TiC/Cu-Al_2O_3 composite deformed at 0.001 s^{-1} strain rate and different temperatures: (a) 450 °C; (b) 650 °C; (c) 850 °C

observed at the higher deformation temperature of 850 °C in Fig. 3(c), which implies that dynamic recrystallization occurs. Since the strain rate of 0.001 s^{-1} is very low and deformation temperature is high, there is enough time for the full recrystallization process and microstructure evolution. Many of the equiaxed grains can be seen in Fig. 3(c).

Microstructure of the composite at 0.001 s^{-1} strain rate and 750 °C deformation temperature is shown in Fig. 4. The grains of the composite deformed at 0.001 s^{-1} in Fig. 4(a) indicate the occurrence of dynamic recrystallization. Since the duration of dynamic recrystallization process is very short and the structural evolution is interrupted as a result of water quenching after hot deformation, dynamic recrystallization is not completely finished and parts of the deformed structure can also be observed. It can be seen that twins and dislocations are present in the deformed composite in Fig. 4(b) and (c). Twins and dislocations increase the strength of materials. Figure 4(d) shows that there is an amorphous layer about 20-30 nm thick between copper and titanium carbide, which helps copper and titanium carbide to bond better and improve the strength.

3.4 Constitutive Equation

In the hot working process, the relationships between the strain rate, deformation temperature and flow stress are expressed by the following equations (Ref 21, 22):

$$\dot{\varepsilon} = A_1 \sigma^n \exp\left(-\frac{Q}{RT}\right) (\alpha\sigma < 0.8) \quad \text{(Eq 1)}$$

$$\dot{\varepsilon} = A_2 \exp(\beta\sigma) \exp\left(-\frac{Q}{RT}\right) (\alpha\sigma > 1.2) \quad \text{(Eq 2)}$$

$$\dot{\varepsilon} = A[\sinh(\alpha\sigma)]^n \exp\left(-\frac{Q}{RT}\right) \text{ (for all stress)} \quad \text{(Eq 3)}$$

Here, A_1, A_2, A, α and β are material's constants, R is the universal gas constant, n is the stress exponent, Q is the activation energy for hot deformation, T is the absolute hot working temperature, and $\dot{\varepsilon}$ is the strain rate. Equation 1 is suitable for low stress, and the exponent-type Eq 2 is suitable for high stress. The hyperbolic sine Eq 3 is suitable for stresses over a wide range.

The relationship between the strain rate, deformation temperature and flow stress was obtained using the Zener–Hollomon parameter, which can be calculated from the equation proposed by Sellars and McTegart (Ref 23, 24):

$$Z = A[\sinh(\alpha\sigma)]^n \quad \text{(Eq 4)}$$

Taking natural logarithms of both sides of Eq 1, 2 and 4 yields:

$$\ln\dot{\varepsilon} = \ln A_1 - \frac{Q}{RT} + n\ln\sigma \quad \text{(Eq 5)}$$

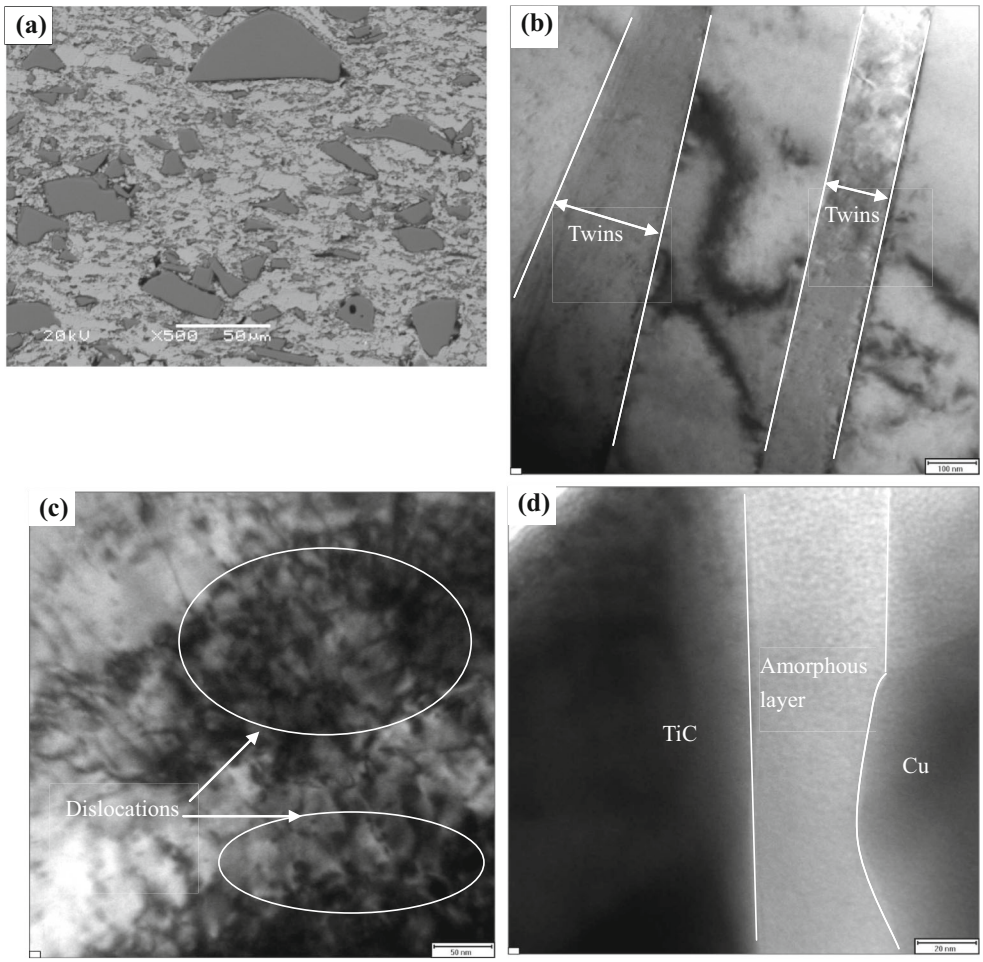

Fig. 4 Microstructure of the 20 vol.% TiC/Cu-Al_2O_3 composite deformed at 750 °C and 0.001 s^{-1} strain rate: (a) SEM image; (b, c, d) HRTEM images

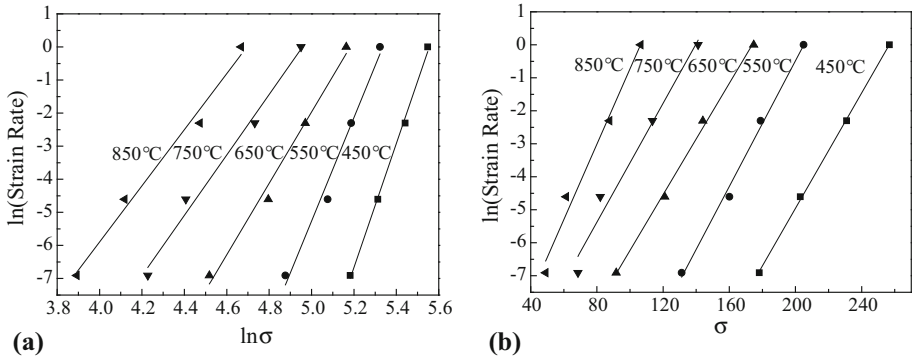

Fig. 5 Relationships between the flow stress and the strain rate: (a) lnσ–ln $\dot{\varepsilon}$ and (b) σ–ln $\dot{\varepsilon}$

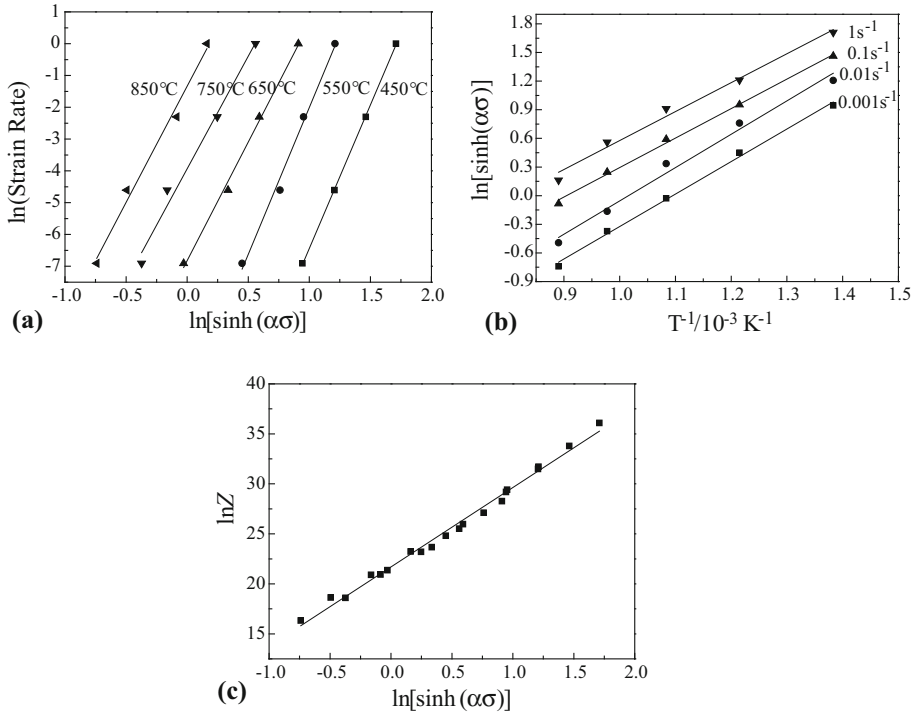

Fig. 6 (a) ln[sinh(ασ)]-ln $\dot{\varepsilon}$; (b) 1000/T-ln[sinh(ασ)]; and (c) ln[sinh(ασ)]-lnZ graphs

$$\ln \dot{\varepsilon} = \ln A_2 - \frac{Q}{RT} + \beta\sigma \qquad \text{(Eq 6)}$$

$$\ln Z = \ln A + n \ln[\sinh(\alpha\sigma)] \qquad \text{(Eq 7)}$$

α can be obtained from lnσ versus ln $\dot{\varepsilon}$ plots and σ versus ln $\dot{\varepsilon}$ plots, shown in Fig. 5, and the value of α is 0.0094.

In order to calculate n and lnA, ln[sinh(ασ)] versus ln $\dot{\varepsilon}$ plots and ln[sinh(ασ)] versus lnZ plots are shown in Fig. 6. The values of n and lnA are 8.0195 and 21.6932, respectively.

$$Q = R\frac{\partial \ln[\sinh(\alpha\sigma)]}{\partial(1/T)}\bigg|_{\dot{\varepsilon}} \frac{\partial \ln \dot{\varepsilon}}{\partial \ln[\sinh(\alpha\sigma)]}\bigg|_{T} = RnS \qquad \text{(Eq 8)}$$

S can be obtained from the $1000/T$ versus ln[sinh(ασ)] plots shown in Fig. 6(b). Thus, S is 3.2543 and Q is 218.9256 kJ/mol. Based on the above analysis, the constitutive equation for the 20 vol.% TiC/Cu-Al_2O_3 composite at high temperature is:

$$\dot{\varepsilon} = e^{21.6932}[\sinh(0.0094\sigma)]^{8.0195} \exp\left(-\frac{218925.6}{8.314T}\right) \qquad \text{(Eq 9)}$$

Yang et al. (Ref 25) studied the thermal deformation behavior of 10% TiC/Cu-Al_2O_3 composite materials and found that the thermal activation energy was 170.73 kJ/mol. The addition of TiC increases the deformation resistance of the material, resulting in an increase in thermal activation energy. Rodrigo et al. (Ref 26) studied the creep behavior of Cu-TiC composites and determined the activation energy of the material at 109-156 kJ/mol. The activation energy is lower than the 20 vol.% TiC/Cu-Al_2O_3 composite material tested in this experiment. This shows that after strengthening the material with Al_2O_3 and TiC, it needs more energy to be deformed.

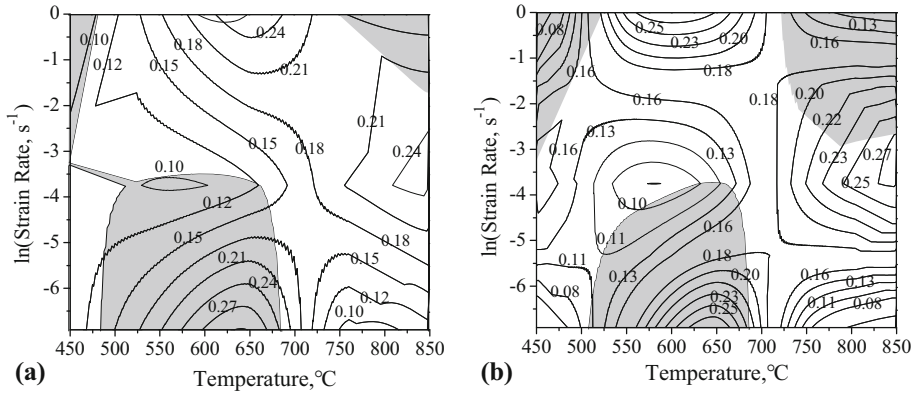

Fig. 7 Processing maps of the 20 vol.% TiC/Cu-Al_2O_3 composite at various true stains: (a) ε = 0.3 and (b) ε = 0.5

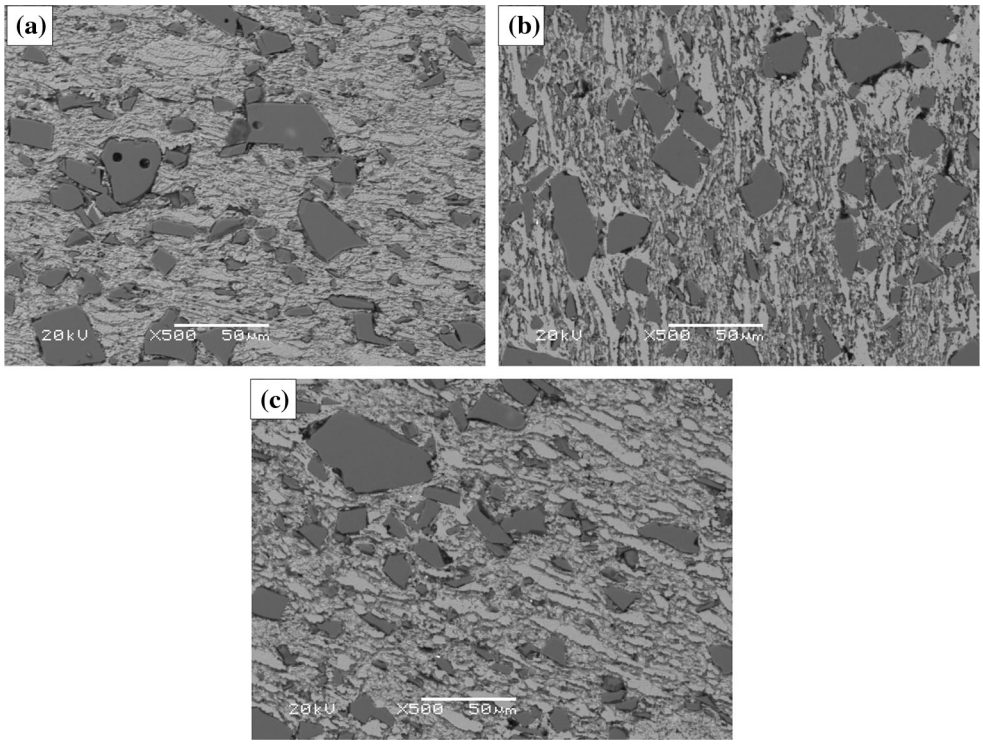

Fig. 8 The microstructure of different regions of the processing map for the 20 vol.% TiC/Cu-Al_2O_3 composite: (a) T = 450 °C, $\dot{\varepsilon}$ = 1 s^{-1}; (b) T = 850 °C, $\dot{\varepsilon}$ = 1 s^{-1}; and (c) T = 750 °C, $\dot{\varepsilon}$ = 0.01 s^{-1}

3.5 Processing Maps

The processing map is an effective tool to design and optimize material's hot working processes. The processing map is constructed by using the principles of the dynamic materials model (DMM) (Ref 27, 28). In this model, material's deformation behavior can be analyzed under different conditions. The hot working process parameters need to be optimized to make sure that hot working is in the "safe" and not in the "unsafe" zone.

Based on the DMM, the processing map of the composite is shown in Fig. 7. The numbers against the contour lines represent percent efficiency of power dissipation, while shaded domains represent unstable regions.

It can be seen that the processing map is clearly divided into stable and unstable domains. The contours represent efficiency of power dissipation in percent, which indicates the microstructure changes during hot deformation. The shaded domains represent the boundaries for instability and cracking, which result from localized deformation. The processing maps at different strains are essentially similar, which indicates that strain does not have a significant role. It can be seen that three instability domains occurred at strains of 0.3 and 0.5. The first region is at the temperature higher than 750 °C and the strain rate higher than 0.1 s^{-1}, the second region is at the temperature lower than 500 °C and the strain rate higher than 0.04 s^{-1}, and the last region is at the temperature ranging from 500 to 670 °C and the strain rate ranging from 0.001 to 0.02 s^{-1}. Simultaneously, the map exhibits domain at the temperature higher than 700 °C and the strain rate ranging from 0.006 to 0.2 s^{-1} with the higher efficiency of about 20%.

At the lower temperature of 450-550 °C and the lower strain rate, the conversion of the energy of deformation into activation energy of dynamic recrystallization is lower because of the lower temperature (Fig. 3a), and part of the dynamic recrystallization occurs in this region. At the lower temperature of 450-550 °C and the higher strain rate, the TiC/Cu-Al_2O_3 composite material will be unstable, as shown in Fig. 8(a). When the temperature is about 750 °C, coupled with the higher strain rate, a long period of time is needed for dynamic recrystallization nucleation and growth. However, for the relatively short deformation time, the effect of work hardening is higher than softening by dynamic recrystallization, thereby forming the unstable region (Fig. 8b). The region with the higher temperature and the lower strain rate is stable region in Fig. 8c. Since the softening rate by dynamic recrystallization is higher than the work hardening rate, the activation energy of thermal deformation converts into dynamic recrystallization. As a result, the optimal processing parameters for hot working occurred at 700-850 °C and 0.001-0.04 s^{-1} strain rate, with 10-27% efficiency of power dissipation.

4. Conclusions

Hot deformation behavior of the 20 vol.% TiC/Cu-Al_2O_3 composite was studied by isothermal compression tests at temperatures ranging from 450 to 850 °C and strain rates ranging from 0.001 to 1 s^{-1}. The main conclusions are summarized as follows.

1. True stress–strain curves of the composite show typical characteristics of dynamic recrystallization. The flow stress decreases with increasing the deformation temperature and decreasing the strain rate. This means that the 20 vol.% TiC/Cu-Al_2O_3 composite belongs to temperature- and strain rate-sensitive materials.
2. The relationship between the strain rate, deformation temperature and flow stress is expressed by the constitutive equation: $\dot{\varepsilon} = e^{21.6932}[\sinh(0.0094\sigma)]^{8.0195}\exp\left(-\frac{218925.6}{8.314T}\right)$, while the activation energy is calculated as 218.9 kJ/mol.
3. The processing maps of the composite have been established. The optimal domain for hot working is at 700-850 °C and 0.001-0.04 s^{-1} strain rate, with 10-27% power dissipation efficiency.

Acknowledgments

This work was supported by the Science and Technology Open Cooperation Fund of the Henan Province. The authors are grateful to Prof. Zhou Xudong for his assistance with the experiment. AV acknowledges support from the National Science Foundation (IRES 1358088).

References

1. A. Chrysanthou and G. Erbaccio, Enhancing the Dispersion of TiC in Copper, *J. Mater. Lett.*, 1996, **15**, p 774–775
2. P.G. Koppad, K.T. Kashyap, V. Shrathinth, T.A. Shetty, and R.G. Koppad, Microstructure and Microhardness of carbon Nanotube Reinforced Copper Nanocomposites, *Mater. Sci. Technol.*, 2013, **29**, p 605–609
3. N. Zarrinfar, A.R. Kennedy, and P.H. Shipway, Reaction Synthesis of Cu–TiCx Master-Alloys for the Production of Copper-Based Composites, *Scripta Mater.*, 2004, **50**, p 949–952
4. Y.H. Liang, H.Y. Wang, Y.F. Yang, Y.Y. Wang, and P.C. Jiang, Evolution Process of the Synthesis of TiC in the Cu–Ti–C System, *J. Alloys Compds.*, 2008, **452**, p 298–303
5. N. Zarrinfar, P.H. Shipway, A.R. Kennedy, and A. Saidi, Carbide Stoichiometry in TiCx and Cu–TiCx Produced by Self-Propagating High-Temperature Synthesis, *Scripta Mater.*, 2002, **46**, p 121–126
6. J.H. Jang, C.H. Lee, H.N. Han, H.K.D.H. Bhadeshia, and D.W. Sun, Modelling Coarsening Behaviour of TiC Precipitates in High Strength, Low Alloy Steels, *Mater. Sci. Technol.*, 2013, **29**, p 1074–1079
7. S. Rathod, O.P. Modi, B.K. Prasad, A. Chrysanthou, D. Vallauri, V.P. Deshmukh, and A.K. Shah, Cast In Situ Cu–TiC Composites: Synthesis by SHS Route and Characterization, *Mater. Sci. Eng. A*, 2009, **502**, p 91–98
8. H.W. Wang, J.Q. Qi, C.M. Zou, and Z.J. Wei, Effect of Microstructural Characteristics on Room Temperature Tensile Properties of In Situ Synthesised TiC/TA15 Composite, *Mater. Sci. Technol.*, 2012, **28**, p 597–602
9. R.H. Palma, A.H. Seputveda, R.A. Espinoza, and R.C. Montiglio, Performance of Cu-Tic Alloy Electrodes Developed by Reaction Milling for Electrical-Resistance Welding, *J. Mater. Process. Technol.*, 2005, **162**, p 62–66
10. F. Ren, A. Zhi, D. Zhang, B. Tian, A.A. Volinsky, and X. Shen, Preparation of Cu-Al2O3 Bulk Nano-Composites by Combining Cu-Al Alloy Sheets Internal Oxidation with Hot Extrusion, *J. Alloys Compd.*, 2015, **633**, p 323–328
11. F. Ren, X. Li, J. Ren, Y. Xiong, A.A. Volinsky, and B. Tian, Precipitated Al_2O_3 Phase Characterization in Internally Oxidized Cu–Al Alloy Sheets, *J. Alloys Compd.*, 2017, **695**, p 452–457
12. Y. Zhang, H. Sun, A.A. Volinsky, B. Tian, Z. Chai, and P. Liu, Characterization of the Hot Deformation Behavior of Cu–Cr–Zr Alloy by Processing Maps, *Acta Metall. Sin.*, 2016, **29**, p 422–430
13. Y. Zhang, H. Sun, A.A. Volinsky, B. Tian, K. Song, and B. Wang, Hot Workability and Constitutive Model of the Cu-Zr-Nd Alloy, *Vacuum*, 2017, **146**, p 35–43
14. Y. Zhang, H. Sun, A.A. Volinsky, B. Wang, B. Tian, and Y. Liu, Constitutive Model for Hot Deformation of the Cu-Zr-Ce Alloy, *J. Mater. Eng. Perform.*, 2018, **27**, p 728–738
15. Y. Zhang, H. Sun, A.A. Volinsky, B. Wang, B. Tian, and Z. Chai, Small Y Addition Effects on Hot Deformation Behavior of Copper-matrix Alloys, *Adv. Eng. Mater.*, 2017, **19**, p 1700197
16. M. Besterci, J. Ivan, L. Kovac, T. Weissgaerber, and C. Sauer, Strain and Fracture Mechanism of Cu–TiC, *Mater. Lett.*, 1999, **38**, p 270–274
17. J.H. Xiong, J.H. Huang, Z.P. Wang, Y.H. Ban, H. Zhang, and X.K. Zhao, Brazing of Carbon Fibre Reinforced SiC Composite and Ti Alloy Using Cu–Ti–C Filler Materials, *Mater. Sci. Technol.*, 2010, **26**, p 356–360
18. C.R. Rambo, M. Travitzky, K. Zimmerman, and P. Greil, Synthesis of TiC/Ti–Cu Composites by Pressureless Reactive Infiltration of TiCu Alloy into Carbon Preforms Fabricated by 3D-Printing, *Mater. Lett.*, 2005, **59**, p 1028–1031
19. L.X. Zhang, J.C. Feng, and H.B. Liu, High Frequency Induction Brazing of TiC Cermets to Steel with Ag–Cu–Zn Foil, *Mater. Sci. Technol.*, 2008, **24**, p 623–626
20. B.H. Tian, P. Liu, K.X. Song, Y. Li, Y. Liu, F.Z. Ren, and J.H. Su, Microstructure and Properties at Elevated Temperature of a Nano-Al_2O_3 Particles Dispersion-Strengthened Copper Base Composite, *Mater. Sci. Eng. A*, 2006, **435**, p 705–710
21. R.X. Chai, D.H. Xu, and C. Guo, Prediction of Constitutive Behaviour of 20CrMnTiH Steel Under Hot Deformation Conditions, *Mater. Sci. Technol.*, 2012, **28**, p 857–863
22. H. Shi, A.J. McLaren, C.M. Sellars, R. Shahani, and R. Bolingbroke, Constitutive Equations for High Temperature Flow Stress of Aluminium Alloys, *Mater. Sci. Technol.*, 1997, **3**, p 210–216
23. C.M. Sellars and W.J. McTegart, On the Mechanism of Hot Deformation, *Acta Metall.*, 1966, **14**, p 1136–1138
24. C. Zener and J.H. Hollomon, Effect of Strain Rate Upon Plastic Flow of Steel, *J. Appl. Phys.*, 1944, **15**, p 22–32
25. Z.Q. Yang, Y. Liu, B.H. Tian, and Y. Zhang, Model of Critical Strain for Dynamic Recrystallization in 10%TiC/Cu-Al_2O_3 Composite, *J. Cent. South Univ.*, 2014, **21**, p 4059–4065

26. R.H. Palma and A.O. Sepúlveda, Creep Behavior of Two Cu-2 vol.% TiC Alloys Obtained by Reaction Milling and Extrusion, *Mater. Sci. Eng. A*, 2013, **588**, p 82–85
27. B.K. Prasad, S.P. Narayan, O.P. Modi, N. Ramakrishnan, A.M. Kumar, and A.K. Sachdev, Microstructure and Micromechanism Maps to Optimise Useful Deformation Processing Conditions in Magnesium Alloy, *Mater. Sci. Technol.*, 2011, **27**, p 1639–1647
28. H.Z. Li, H.J. Wang, X.P. Liang, H.T. Liu, Y. Liu, and X.M. Zhang, Hot Deformation and Processing Map of 2519A Aluminum Alloy, *Mater. Sci. Eng. A*, 2011, **528**, p 1548–1552